The Astrophysical Journal Letters, 941:L26 (6pp), 2022 December 20 https://doi.org/10.3847/2041-8213/aca673

Polytropic Behavior in the Structures of Interplanetary Coronal Mass Ejections

M. A. Dayeh[1,2] and G. Livadiotis[3]
[1] Southwest Research Institute, San Antonio, TX 78238, USA; maldayeh@swri.edu
[2] University of Texas at San Antonio, San Antonio, TX 78249, USA
[3] Princeton University, Princeton, NJ 08544, USA
Received 2022 September 21; revised 2022 November 20; accepted 2022 November 28; published 2022 December 16

Abstract

The polytropic process characterizes the thermodynamics of space plasma particle populations. The polytropic index, γ, is particularly important as it describes the thermodynamic behavior of the system by quantifying the changes in temperature as the system is compressed or expanded. Using Wind spacecraft plasma and magnetic field data during 1995 February–2015 December, we investigate the thermodynamic evolution in 336 interplanetary coronal mass ejection (ICME) events. For each event, we derive the index γ in the sheath and magnetic ejecta structures, along with the pre- and post-event regions. We then examine the distributions of all γ indices in these four regions and derive the entropic gradient of each, which is indicative of the ambient heating. We find that in the ICME sheath region, where wave turbulence is expected to be highest, the thermodynamics takes longest to recover into the original quasi-adiabatic process, while it recovers faster in the quieter ejecta region. This pattern creates a thermodynamic cycle, featuring a near adiabatic value $\gamma \sim \gamma_a$ (=5/3) upstream of the ICMEs, $\gamma_a - \gamma \sim 0.26$ in the sheaths, $\gamma_a - \gamma \sim 0.13$ in the ICME ejecta, and recovers again to $\gamma \sim \gamma_a$ after the passage of the ICME. These results expose the turbulent heating rates in the ICME plasma: the lower the polytropic index from its adiabatic value and closer to its isothermal value, the larger the entropic gradient, and thus, the rate of turbulent heating that heats the ICME plasma.

Unified Astronomy Thesaurus concepts: Solar coronal mass ejections (310); Space plasmas (1544); Polytropes (1281)

1. Introduction

Coronal mass ejections (CMEs) are gigantic eruptions of magnetized plasma structures from the Sun (e.g., Gopalswamy 2006; Webb & Howard 2012; Dayeh 2015; Kilpua et al. 2019) that propagate in the interplanetary (IP) space to reach far into the outer heliosphere (e.g., Wang et al. 2001; Richardson 2006; Liu et al. 2014). Once away from the Sun, CMEs evolve into interplanetary CMEs (ICMEs). ICMEs that are sufficiently faster than the ambient solar wind tend to drive an IP shock. These IP shocks can accelerate IP particles to high energies, often contributing to solar energetic particle events associated with CME eruptions. A nominal ICME comprises two major parts: (i) a sheath—a region of shocked, heated, and inhomogeneous plasma that exhibits high turbulence levels and variability of plasma physical processes (e.g., Kilpua et al. 2019) and (ii) a magnetic obstacle (MO)—a solar wind structure that is often associated with enhanced magnetic field, smooth rotation, suppressed proton temperature, and is thought to be a flux rope with reduced turbulence (e.g., Burlaga et al. 1981). ICME sheaths are key drivers of geomagnetic activity at Earth, leading to intense space weather consequences (Tsurutani et al. 1988). Enhanced sheath turbulence can particularly intensify the geomagnetic activity (e.g., Borovsky & Funsten 2003). Furthermore, ICME-driven shocks can accelerate suprathermal particles (Dayeh et al. 2009, 2017) to very high energies (10 s of MeV) and are often associated with very large enhancements of particles, known as energetic storm particle (ESP) events (e.g., Desai et al. 2003; Cohen 2006; Dayeh et al. 2018). Both ESPs and ICME geomagnetic effectiveness are key elements of space weather. Understanding ICME propagation and internal processes is thus an important aspect to further advance our space weather capabilities.

Remote observations of CMEs close to the Sun have provided insights into the heating and acceleration processes of the embedded plasma. Studies using Solar and Heliospheric Observatory spacecraft extreme ultraviolet (EUV) measurements showed that CMEs ambient temperatures are higher than the ambient solar wind, suggesting that the inner corona transfers thermal energy into the CME plasma (Kohl et al. 2006; Bemporad & Mancuso 2010; Mishra et al. 2020). On the other hand, in situ measurements of ICMEs have provided a plethora of information about ICME plasma properties and evolution. Compared to the ambient solar wind, in situ observations from missions across the heliosphere (Voyagers: >1 au–>100 au; Ulysses: 5 au; Helios: <1 au; WIND: 1 au; ACE: 1 au; STEREO: 1 au) provided direct evidence that ICMEs have lower temperatures (Burlaga et al. 1981; Richardson & Cane 1993) and highly elevated ionic charge states (Lepri et al. 2001; Zurbuchen et al. 2003). The latter is an indicative of strong heating at the CME source in the lower corona.

Thermodynamic properties of ICMEs can be studied using a polytropic state estimation. Polytropic behavior defines specific relations among thermodynamical observables such as plasma density and temperature. In numerous cases, space plasma density and temperatures positively correlate with different values of the polytropic index, γ, and thus indicate different thermodynamical states (e.g., Totten et al. 1995; Nicolaou et al. 2014; Livadiotis & Desai 2016).

The polytropic relationship may be expressed by

$$P \cdot n^{-\gamma} = T \cdot n^{1-\gamma} = \text{const.}, \quad (1)$$

which involves the thermal pressure P, the temperature T, and the density n of the plasma. The polytropic expression for the logarithms of the thermal variables becomes linear and allows a straightforward estimation of the polytropic index γ by examining data sets of $\log(T)$ versus $\log(n)$.

Variations in γ among ICME structures are indicative of heating processes. Evolution of these processes in time and space as the ICME expands (e.g., Lugaz et al. 2020) can be studied in radially aligned spacecraft over different distances in the heliosphere (e.g., Phillips et al. 1995; Skoug et al. 2000). It is important to note that studying thermodynamical properties as function of radial distance from the Sun is a key approach to understand the ICME physical properties and heating processes. Thus, analysis of an ensemble is required to draw physical conclusions on the evolution of the thermodynamical properties from a single location.

Statistical studies at different distances from the Sun have shown that as a function of radial distance away from the Sun and compared to the ambient solar wind, proton density and magnetic field magnitudes decrease at a faster rate in ICMEs, while the temperature drops at a slower rate, indicating that the expansion of ICMEs in the IP space is closer to an isothermal process (e.g., Wang & Richardson 2004; Liu et al. 2005; Wang et al. 2005; Liu et al. 2006; Mishra et al. 2020). Using combined surveys of ICMEs between 0.3 and 20 au, Liu et al. (2006) showed that ICMEs expand moderately in the solar wind and are governed by an averaged polytropic index of $\sim$1.3. The authors suggested that turbulence dissipation seems sufficient to explain the observed ICME heating.

In this work, we examine the polytropic behavior and the change of entropy in four different regions, representing before, during, and after the passage of 336 ICMEs measured at 1 au, and then, connect the evolution of the polytropic behavior and the corresponding thermodynamic states to the heating of the ICME plasma. We find that ICMEs exhibit a thermodynamic cyclic behavior that expose the turbulent heating rates in the ICME; the lower the polytropic index from its adiabatic value and closer to its isothermal one, the larger the rate of turbulent energy that heats the ICME plasma. We organize the Letter as follows. Sections 2 and 3 describe the data used and the methodology followed by our analysis. The results are shown in Section 4. Finally, Section 5 summarizes and discusses the results.

2. Data

Events in this study are from the Wind ICME catalog compiled by Nieves-Chinchilla et al. (2018). It covers the period from 1995 February to 2015 December and expands on extensive previous ICME catalogs (Nieves-Chinchilla et al. 2005; Jian 2006; Richardson & Cane 2010; Kilpua 2011; Lepping 2011, 2015) and publicly available lists. The catalog comprises 337 ICMEs that exhibit clear signatures of an organized magnetic structure of an IP shock, sheath region, followed by a magnetic obstacle that is composed of one or more flux ropes. Timings for the shock arrival, the sheath, and the magnetic obstacle are provided. We exclude one event where plasma parameters are not available, resulting in 336 ICMEs for this study . We also use high cadence solar wind plasma, derived plasma moments, and magnetic field measurements from the Solar Wind Experiment (Ogilvie et al. 1995) and the Magnetic Field Investigation (Lepping et al. 1995) on board Wind. Data is obtained from the Coordinated Data Analysis Web (CDAWeb).

Figure 1 shows one of the events and the four regions of interest, namely, the ICME sheath and magnetic ejecta structures, along with the pre- and post-event regions. Shown are the (a) protons' speed, (b) and (c) magnetic field components and magnitude, (d) proton number density, and (e) the proton thermal speed. The sharp jump in the magnetic field indicates the arrival of the ICME-driven shock followed by the magnetically turbulent sheath region, which in turn is followed by the magnetic obstacle demonstrated by the slow rotation of the magnetic field.

3. Methodology

The methodology of deriving the polytropic indices is summarized in the following steps, which are also illustrated in Figure 2. Details of this method and its sensitivity has also been substantiated in previous analyses, e.g., Kartalev et al. (2006), Nicolaou et al. (2014), Livadiotis (2018a), Nicolaou & Livadiotis (2019).

1. *Time intervals.* We use a sequence of a 5 minute moving window comprising five data points. This approach is validated and aims at minimizing mixed particle measurements on different streamlines (Figure 2(a)).
2. *Data filtration.* For each selected interval, we examine the stability of Bernoulli's integral by requiring the variance over the mean to be less than 10%. This condition is particularly important, as it ensures that γ is derived for likely-the same plasma ensemble along the same streamline. (Figure 2(a); not shown).
3. *Density–Temperature fitting.* We fit a linear model to the data plot of $\log(T)$ versus $\log(n)$ to infer the value of γ (Equation (1); Figure 2(b)).
4. *Determining γ.* Repeating step 3 for all time windows in any region results in a set of polytropic indices, from which the mean can then be determined (Figure 2(c)).

We derive the polytropic index in four regions associated with each ICME event, namely, pre-ICME (1 day prior to shock arrival), sheath, magnetic obstacle, and post-ICME (1 day after), as illustrated in Figure 1. We further constrain the selection of the events to comply with the following criteria: all the examined four regions (pre-ICME solar wind, sheath, magnetic obstacle/ejecta, and post-ICME solar wind) have to be characterized by a derived value of the polytropic index γ; then, the polytropic indices of a region are only accepted if they are statistically significant: more than 10 derived values of polytropic index, with standard deviation less than the 20% of the respective mean; there must be no statistical significant trend of the derived polytropic indices with speed (e.g., Livadiotis & Desai 2016; Livadiotis 2018b; Livadiotis et al. 2018). Among all the studied events (336), we have selected 25 "clean" events that follow the aforementioned criteria. These events are listed in Table 1. Two of these had complex structures in the pre-ICME period (event 12) and the post-ICME period (event 21), which is probably the reason why the inferred γ was high during these times. Note that such complexities may include other solar transient structures. For instance, ICME-driven shocks can propagate into preceding ICME structures (e.g., Burlaga et al. 1987), and the preceding

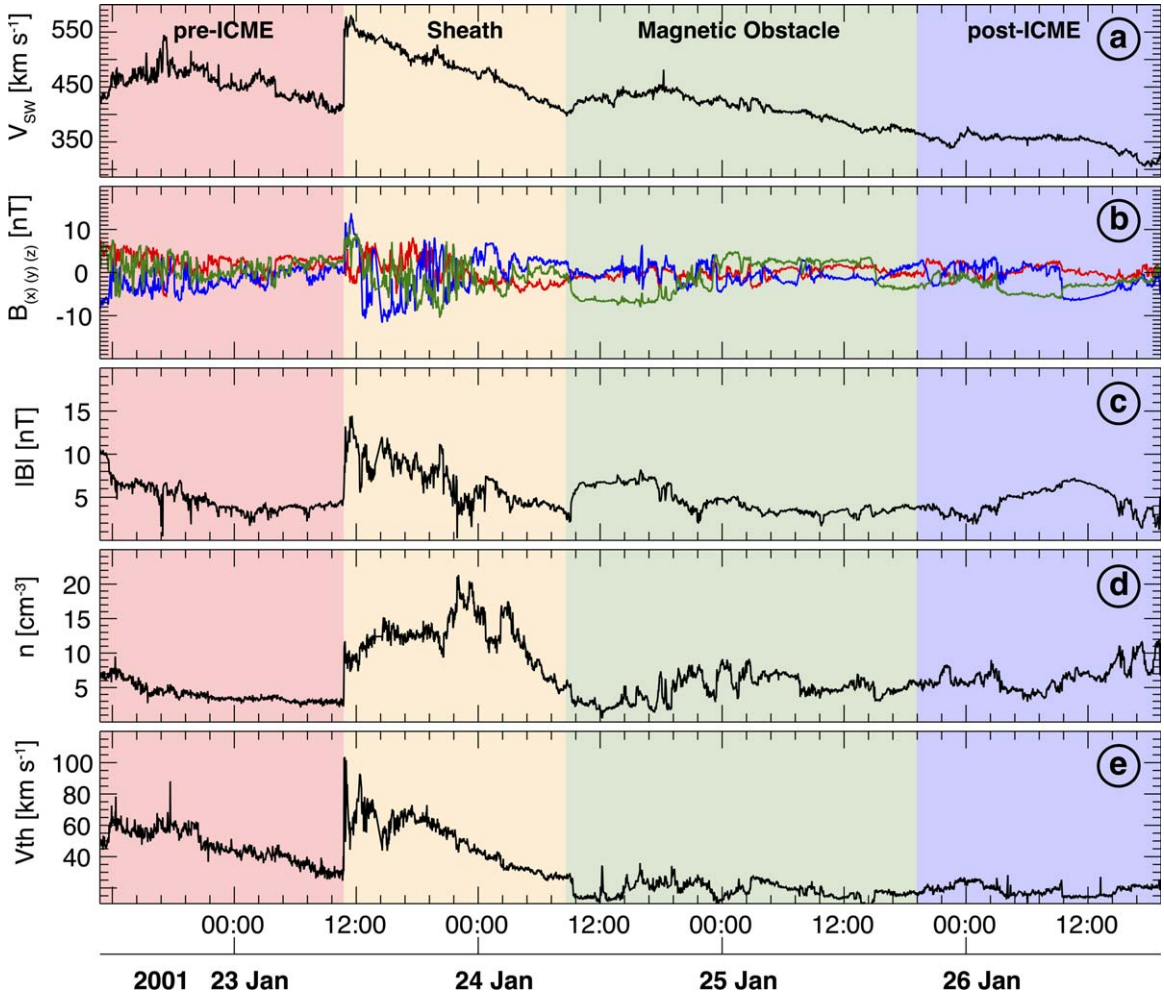

Figure 1. Time series of plasma parameters showing an ICME and the four examined regions highlighted as pre-ICME (pink), sheath (light brown), magnetic obstacle (green), and post-ICME (purple). (a) Proton speed, (b) Magnetic field components, (c) magnetic field magnitude, (d) proton number density, and (e) proton thermal speed.

ICME could be completely stuck in the sheath region of the following ICME—a phenomenon termed an "ICME-in-sheath" (e.g., Liu et al. 2020). These complexities alter the thermodynamical properties of their corresponding time periods.

4. Results

Figure 3 shows the histograms of all the derived polytropic indices in the four studied regions (green), and those of the "clean" selected events (yellow). The enriched histograms of the selected events are also shown. The enriched histograms are specifically constructed so that both the binned values and their uncertainties are taken into account.

The histogram of a set of values is not reliable if these are characterized by highly varying uncertainties. In this case, we construct the enriched histograms. For each point value and its uncertainty, we generate a normally distributed set of 10^3 values, with a mean and sigma values corresponding to the original value and its uncertainty. This effectively changes the distribution of original values in which their uncertainties were not considered (further details on the technique are described in Livadiotis 2016).

Next, we connect the derived polytropic indices with the entropy gradient (Adhikari et al. 2020; Livadiotis et al. 2020) and the turbulent heating gradient (Verma et al. 1995; Vasquez et al. 2007; Livadiotis 2019, 2021). Combining the entropy expressed in terms of temperature and density

$$\frac{1}{k_B}S = \ln W \text{ with } W \propto T^{d_{eff}/2}/n, \tag{2}$$

the polytropic relationship between temperature and density

$$T \propto n^{\gamma-1}, \tag{3}$$

and the density drop due to the CME expansion can be approximated as

$$n \propto R^{-2}, \tag{4}$$

we find

$$\frac{1}{k_B}S = d_{\text{eff}} \cdot (\gamma_a - \gamma) \cdot \ln R + \text{const.}, \tag{5}$$

where the adiabatic polytropic index can be written in terms of the effective kinetic degrees of freedom, $\gamma_a = 1 + 2/d_{\text{eff}}$ (Livadiotis 2015), so that, $\gamma_a \sim 5/3$, for $d_{\text{eff}} \sim 3$, though these values can be affected by the magnetic field direction (Nicolaou & Livadiotis 2019) and magnitude (Livadiotis & Nicolaou 2021).

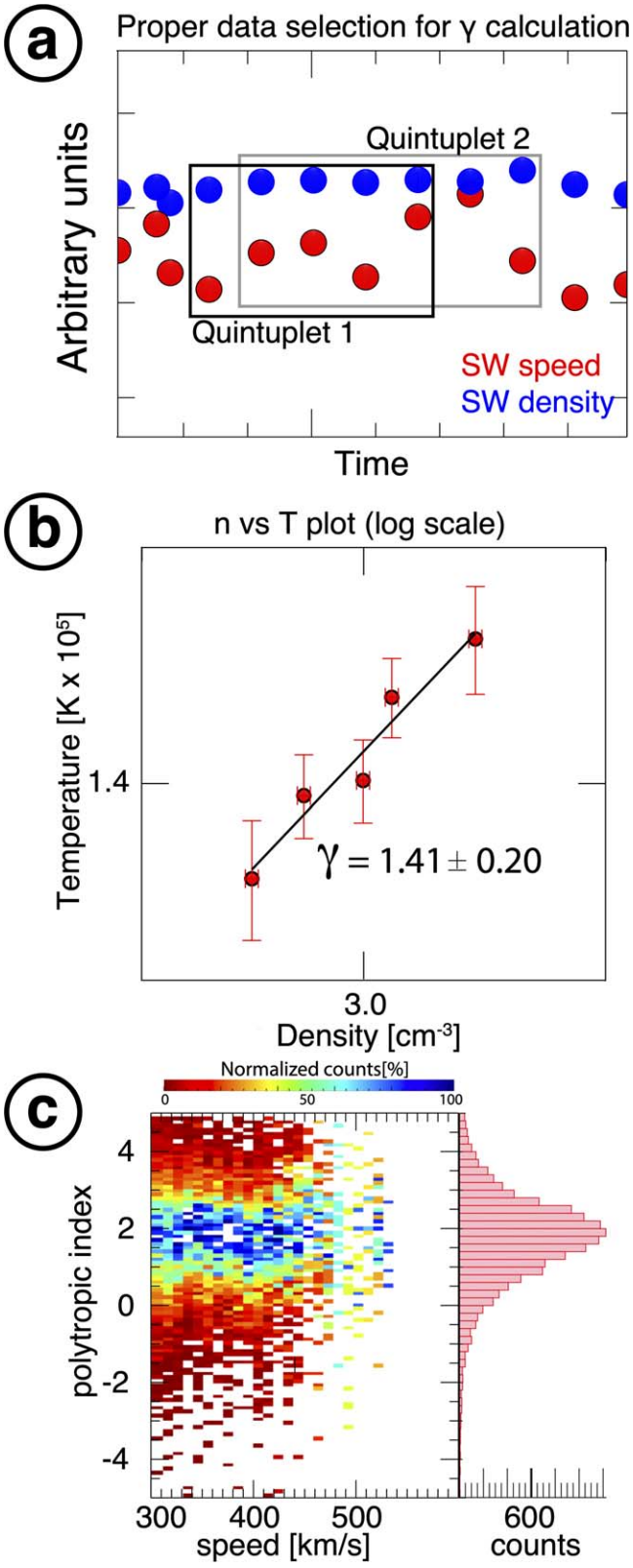

Figure 2. (a) Illustration of the solar wind selection when calculating the polytropic index (see text for details). (b) Temperature vs. density plotted on a log-log scale, where the polytropic index is given as slope = γ-1. (c) Derived polytropic indices are plotted against the solar wind speed in a two-dimensional histogram. This spectrogram is normalized to the number of solar wind velocity bins (see Livadiotis & Desai 2016). The distribution of the polytropic indices is shown on the right.

Then, the entropy gradient becomes

$$\frac{d}{d\ln R}\left(\frac{1}{k_B}S\right) = d_{\rm eff}\cdot(\gamma_a-\gamma). \tag{6}$$

Moreover, the gradient of the turbulent heating E_t of the proton plasma (per mass), normalized by the thermal energy, is also equal to the deviation of the polytropic index γ from its adiabatic value γ_a (Verma et al. 1995; Vasquez et al. 2007; Livadiotis 2019), i.e.,

$$\frac{1}{k_B T}\cdot\frac{dE_t}{d\ln R} = d_{\rm eff}\cdot(\gamma_a-\gamma). \tag{7}$$

Combining the last two formulae together, we conclude in

$$\frac{1}{k_B T}\cdot\frac{dE_t}{d\ln R} = \frac{d}{d\ln R}\left(\frac{1}{k_B}S\right) = d_{\rm eff}\cdot(\gamma_a-\gamma). \tag{8}$$

The CMEs' sheath is highly turbulent compared to the ICMEs' ejecta or the solar wind plasma (Kilpua et al. 2019). This should be also captured in the thermodynamics of ICMEs. According to Equation (1), the entropy is expected to increase and the polytropic index to decrease with increasing the turbulent heating. In particular, for $R\sim 1$ au, the entropic gradient is $\sim 3(\gamma_a-\gamma)$.

Ejecta is less turbulent CME regions; thus, thermodynamics is expected to recover to the original quasi-adiabatic process once the ejecta region is passed. The results shown in Figure 3(b) exactly verify this thermodynamic cycle: $\gamma\sim\gamma_a$ upstream of the ICME, $\gamma_a-\gamma\sim 0.26$ at the sheath, $\gamma_a-\gamma\sim 0.13$ at the ejecta, and again, $\gamma\sim\gamma_a$ at the end of the ICME. The respective entropic gradient dS/dR is 0, 0.78 [k_B/au], 0.39 [k_B/au], and 0.39 [k_B/au], corresponding to entropic gradient jumps $\Delta(dS/dR) = +0.78$ [k_B/au], -0.39 [k_B/au], and -0.39 [k_B/au].

5. Discussion and Conclusions

Polytropic index, entropic gradient, and turbulent heating, all vary before, during, and after the passage of ICMEs at 1 au, revealing a cyclic behavior. In particular, the sheath is characterized by a low polytropic index, which deviates sharply from the adiabatic value prior to the ICME arrival at the spacecraft. Then, the index recovers and increases slightly during the ejecta passage and fully recovers to the pre-ICME levels after the ICME passes by.

Observational results of ICMEs at multiple spacecraft revealed that the sheath expands at a much faster rate (~factor of 2) than that of the ejecta within 1 au (e.g., Lugaz et al. 2020). The polytropic index characterizes compressions or expansions in the system and equivalently heat transfer processes. Although, dissipation of turbulence is not necessarily related to the polytropic process and is intrinsically different (Goldstein et al. 1995), turbulence levels are higher in the sheath, and the contribution of turbulence in altering the polytropic index cannot be ruled out. The observed faster expansion of the sheath may thus naturally correspond to an increased energy absorption, resulting in a low polytropic index.

Table 1
Selected 25 ICME Events that Showed a Statistically Significant Inference of γ

	Pre-ICME		[a]ICME Sheath		[a]ICME Magnetic Obstacle		Post-ICME	
	Time Range	γ_{pre} (σ_γ)	Start-Stop Time	γ_S (σ_γ)	Start-Stop Time	γ_{MO} (σ_γ)	Stop Time	γ_{post} (σ_γ)
1	24 hr prior to the sheath start time	1.75(0.07)	1995 Feb 7 19:11–Feb 8 03:21	1.31(0.04)	1995 Feb 8 03:21–Feb 10 21:36	1.01(0.08)	24 hr after the MO stop time	1.71(0.04)
2		1.37(0.05)	1995 Mar 4 00:36–Mar 4 11:23	1.31(0.05)	1995 Mar 4 11:23–Mar 5 03:06	0.93(0.07)		1.64(0.04)
3		1.86(0.05)	1995 Jun 30 09:21–Jun 30 14:23	1.21(0.03)	1995 Jun 30 14:23–Jul 2 16:47	1.01(0.07)		1.38(0.06)
4		1.36(0.05)	1996 Jul 1 13:05–Jul 1 17:16	1.37(0.05)	1996 Jul 1 17:16–Jul 2 10:17	1.38(0.09)		1.72(0.04)
5		1.18(0.05)	1997 Feb 9 12:50–Feb 10 02:52	1.70(0.06)	1997 Feb 10 02:52–Feb 10 18:28	1.44(0.05)		1.39(0.05)
6		1.63(0.05)	1997 Jun 8 15:43–Jun 9 06:18	1.41(0.08)	1997 Jun 9 06:18–Jun 9 23:01	1.32(0.08)		1.79(0.05)
7		1.63(0.05)	1997 Aug 3 10:10–Aug 3 13:55	1.31(0.05)	1997 Aug 3 13:55–Aug 4 02:23	1.23(0.05)		1.34(0.04)
8		1.75(0.04)	1997 Oct 10 03:08–Oct 10 15:33	1.52(0.05)	1997 Oct 10 15:33–Oct 11 22:00	1.44(0.07)		1.80(0.05)
9		2.30(0.05)	2000 Oct 12 22:33–Oct 13 18:24	1.48(0.05)	2000 Oct 13 18:24–Oct 14 19:12	1.41(0.05)		1.88(0.04)
10		1.81(0.05)	2001 Jan 23 10:47–Jan 24 08:38	1.51(0.04)	2001 Jan 24 08:38–Jan 25 19:12	1.40(0.04)		1.62(0.04)
11		1.71(0.06)	2001 Apr 21 15:29–Apr 22 00:28	1.35(0.06)	2001 Apr 22 00:28–Apr 23 01:11	1.04(0.04)		1.56(0.05)
12		2.56(0.03)	2001 Oct 28 03:13–Oct 29 16:19	1.84(0.08)	2001 Oct 29 16:19–Oct 30 10:47	1.50(0.04)		1.62(0.09)
13		1.91(0.03)	2002 Aug 18 18:40–Aug 19 19:12	1.33(0.05)	2002 Aug 19 19:12–Aug 21 13:25	1.51(0.06)		1.49(0.07)
14		1.70(0.06)	2003 Aug 4 20:23–Aug 5 01:10	1.72(0.05)	2003 Aug 5 01:10–Aug 6 02:23	1.47(0.07)		1.80(0.04)
15		2.02(0.07)	2004 Aug 29 09:09–Aug 29 19:26	1.48(0.03)	2004 Aug 29 19:26–Aug 30 21:21	1.71(0.07)		1.21(0.05)
16		1.86(0.05)	2010 May 28 01:55–May 28 19:12	1.50(0.04)	2010 May 28 19:12–May 29 17:58	1.42(0.05)		2.01(0.03)
17		1.65(0.05)	2010 Oct 31 02:09–Oct 31 05:16	1.63(0.05)	2010 Oct 31 05:16–Nov 1 20:38	1.39(0.05)		1.95(0.04)
18		1.70(0.04)	2011 Oct 24 17:41–Oct 25 00:21	1.58(0.05)	2011 Oct 25 00:21–Oct 25 23:31	1.37(0.11)		2.10(0.06)
19		0.80(0.11)	2012 May 16 12:28–May 16 16:04	1.49(0.05)	2012 May 16 16:04—May 18 02:11	1.36(0.11)		1.97(0.07)
20		1.55(0.05)	2012 Aug 12 12:37–Aug 12 19:12	2.20(0.04)	2012 Aug 12 19:12–Aug 13 05:01	1.51(0.07)		2.10(0.05)
21		1.70(0.06)	2012 Nov 12 22:12–Nov 13 08:23	1.39(0.07)	2012 Nov 13 08:23–Nov 14 08:09	1.49(0.05)		2.47(0.10)
22		1.94(0.05)	2013 Jul 4 17:17–Jul 5 04:05	1.77(0.03)	2013 Jul 5 04:05–Jul 7 14:24	1.37(0.07)		2.01(0.09)
23		1.58(0.06)	2014 Jun 7 16:30–Jun 8 19:12	1.77(0.05)	2014 Jun 8 19:12–Jun 10 16:46	1.18(0.01)		1.65(0.06)
24		1.63(0.06)	2014 Jun 29 16:47–Jun 29 20:53	1.86(0.05)	2014 Jun 29 20:53–Jun 30 11:15	1.55(0.11)		1.68(0.06)
25		1.59(0.04)	2015 Dec 19 15:35–Dec 20 13:40	1.66(0.04)	2015 Dec 20 13:40–Dec 21 23:02	1.18(0.10)		1.52(0.05)

Note.
[a] From Nieves-Chinchilla et al. (2018).

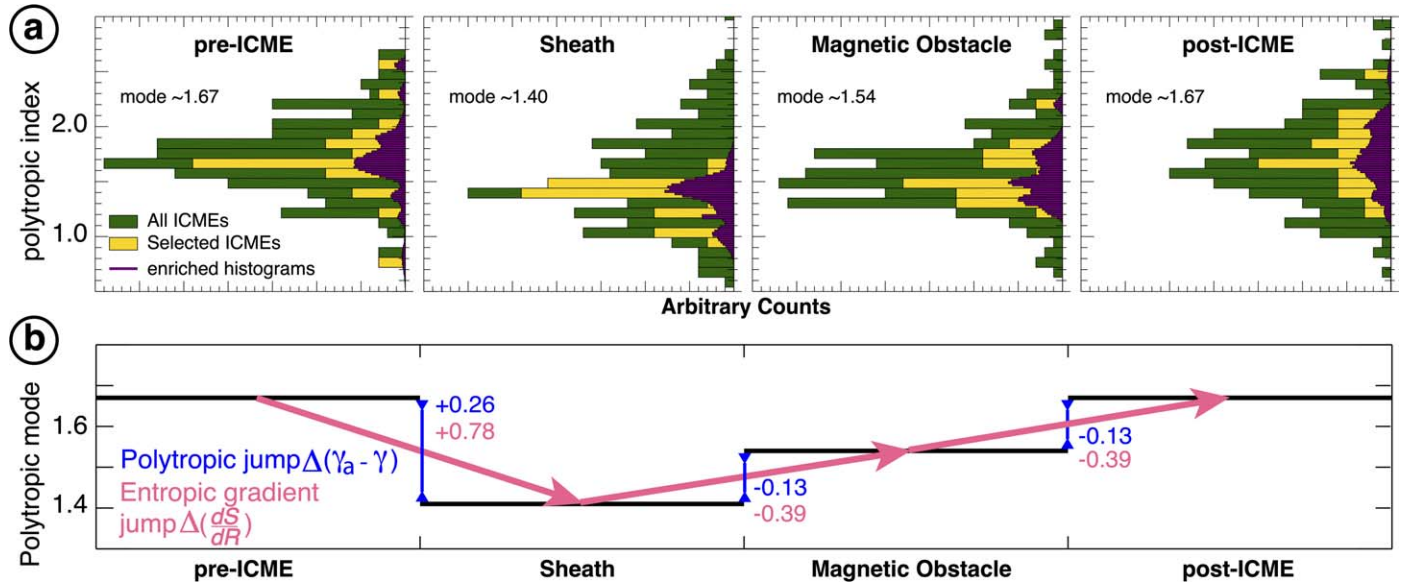

Figure 3. (a) Histograms of all the events (green), of the selected events (yellow), and of the enriched data set of the good events (purple); modes are indicated and histograms are plotted for each region. (b) Calculated "jumps" of the polytropic modes and entropic gradients for R=1 au according to Equation (6).

M.A.D. acknowledges support from NASA LWS grants 80NSSC19K0079, 80NSSC21K1307, SWO2R awards 80NSSC20K0290, and 80NSSC21K0027, and PSP GI award 80NSSC21K1769. M.A.D. and G.L. acknowledge support from the IBEX mission under grants 80NSSC18K0237 and 80NSSC20K0719.

ORCID iDs

M. A. Dayeh https://orcid.org/0000-0001-9323-1200
G. Livadiotis https://orcid.org/0000-0002-7655-6019

References

Adhikari, L., Zank, G. P., Zhao, L.-L., & Webb, G. M. 2020, ApJ, 891, 34
Bemporad, A., & Mancuso, S. 2010, ApJ, 720, 130
Borovsky, J. E., & Funsten, H. O. 2003, JGR, 108, 1246
Burlaga, L., Sittler, E., Mariani, F., & Schwenn, R. 1981, JGR, 86, 6673
Burlaga, L. F., Behannon, K. W., & Klein, L. W. 1987, JGR, 92, 5725
Cohen, C. M. S. 2006, in Solar Eruptions and Energetic Particles, ed. N. Gopalswamy, R. Mewaldt, & J. Torsti, Vol. 165 (New York: Wiley), 275
Dayeh, M. A. 2015, in Handbook of Cosmic Hazards and Planetary Defense, ed. J. N. Pelton & F. Allahdadi (Berlin: Springer), 1
Dayeh, M. A., Desai, M. I., Dwyer, J. R., et al. 2009, ApJ, 693, 2
Dayeh, M. A., Desai, M. I., Ebert, R. W., et al. 2018, JPhCS, 1100, 012008
Dayeh, M. A., Desai, M. I., Mason, G. M., et al. 2017, ApJ, 835, 155
Desai, M. I., Mason, G. M., Dwyer, J. R., et al. 2003, ApJ, 588, 1149
Goldstein, M. L., Roberts, D. A., & Matthaeus, W. H. 1995, ARA&A, 33, 283
Gopalswamy, N. 2006, SSR, 124, 145
Jian, L., Russell, C. T., Luhmann, J. G., et al. 2006, SoPh, 239, 393
Kartalev, M., Dryer, M., Grigorov, K., & Stoimenova, E. 2006, JGR, 111, A10107
Kilpua, E. K. J., Fontaine, D., Moissard, C., et al. 2019, SpWea, 17, 1257
Kilpua, E. K. J., Lee, C. O., Luhmann, J. G., & Li, Y. 2011, AnGeo, 29, 1455
Kohl, J. L., Noci, G., Cranmer, S. R., & Raymond, J. 2006, AAR, 13, 31
Lepping, R. P., Acuna, M. H., Burlaga, L. F., et al. 1995, in The Global Geospace Mission, ed. R. C. T. Kluwer (Dordrecht: Kluwer)
Lepping, R. P., Wu, C.-C., Berdichevsky, D. B., & Szabo, A. 2011, SoPh, 274, 345
Lepping, R. P., Wu, C.,-C., Berdichevsky, D. B., & Szabo, A. 2015, SoPh, 290, 2265
Lepri, S. T., Zurbuchen, T. H., Fisk, L. A., et al. 2001, JGR, 106, 29231
Liu, Y., Richardson, J. D., & Belcher, J. W. 2005, P&SS, 53, 3
Liu, Y., Richardson, J. D., Belcher, J. W., et al. 2006, JGRA, 111, A01102
Liu, Y., Richardson, J. D., Wang, C., & Luhmann, J. G. 2014, ApJL, 788, L28
Liu, Y. D., Chen, C., & Zhao, X. 2020, ApJL, 897, L11
Livadiotis, G. 2015, ApJ, 809, 111
Livadiotis, G. 2016, ApJS, 223, 13
Livadiotis, G. 2018a, JGR, 123, 1050
Livadiotis, G. 2018b, Entr, 20, 799
Livadiotis, G. 2019, Entr, 21, 1041
Livadiotis, G. 2021, RNAAS, 5, 4
Livadiotis, G., Dayeh, M., & Zank, G. P. 2020, ApJ, 905, 137
Livadiotis, G., & Desai, M. I. 2016, ApJ, 829, 88
Livadiotis, G., Desai, M. I., & Wilson, L. B., III 2018, ApJ, 853, 142
Livadiotis, G., & Nicolaou, G. 2021, ApJ, 909, 127
Lugaz, N., Winslow, R. M., & Farrugia, C. J. 2020, JGRA, 125, e27213
Mishra, W., Wang, Y., Teriaca, L., Zhang, J., & Chi, Y. 2020, FrASS, 7, 1
Nicolaou, G., & Livadiotis, G. 2019, ApJ, 884, 52
Nicolaou, G., Livadiotis, G., & Moussas, X. 2014, SoPh, 289, 1371
Nieves-Chinchilla, T., Hidalgo, M. A., & Sequeiros, J. 2005, SoPh, 232, 105
Nieves-Chinchilla, T., Vourlidas, A., Raymond, J. C., et al. 2018, SoPh, 293.2, 25
Ogilvie, K. W., Chornay, K. W., Fritzenreiter, R. J., et al. 1995, in The Global Geospace Mission, ed. C. T. Russell (Dordrecht: Kluwer)
Phillips, K. J. H., Pike, C. D., Lang, J., et al. 1995, AdSpR, 15, 33
Richardson, I. G., & Cane, H. V. 1993, JGR, 98, 15295
Richardson, I. G., & Cane, H. V. 2010, SoPh, 264, 189
Richardson, J. D., Liu, Y., Wang, C., et al. 2006, GRL, 33, L23107
Skoug, R. M., Feldman, W. C., Gosling, J. T., et al. 2000, JGR, 105, 23069
Totten, T. L., Freeman, J. W., & Arya, S. 1995, JGR, 100, 13
Tsurutani, B. T., Gonzalez, W. D., Tang, F., et al. 1988, JGR, 93, 8519
Vasquez, B. J., Smith, C. W., Hamilton, K., et al. 2007, JGR, 112, A07101
Verma, M. K., Roberts, D. A., & Goldstein, M. L. 1995, JGR, 100, 19839
Wang, C., Du, D., & Richardson, J. D. 2005, JGRA, 110, A10107
Wang, C., & Richardson, J. D. 2004, JGR, 109, A06104
Wang, C., Richardson, J. D., & Paularena, K. I. 2001, JGR, 106, 13007
Webb, D. F., & Howard, T. A. 2012, LRSP, 9, 3
Zurbuchen, T. H., Fisk, L. A., Lepri, S. T., et al. 2003, in AIP Conf. Proc. 679, Solar Wind Ten, ed. M. Velli, R. Bruno, & F. Malara (Melville, NY: AIP), 604